Projection of Precipitation Extremes and Flood Risk in the China–Pakistan Economic Corridor

Shixiong Du[1], Ruiying Wu[1,2], Huaiwei Sun[1]*, Dong Yan[1], Jie Xue[3]*, Weihong Liao[4], Ye Tuo[5] and Wenxin Zhang[6]

[1]School of Civil and Hydraulic Engineering, Huazhong University of Science and Technology, Wuhan, China, [2]Water Conservancy Information and Propaganda Education Center, Yancheng, China, [3]State Key Laboratory of Desert and Oasis Ecology, Xinjiang Institute of Ecology and Geography, Chinese Academy of Sciences, Urumqi, China, [4]China Institute of Water Resources and Hydropower Research, Beijing, China, [5]Chair of Hydrology and River Basin Management, Technical University of Munich, Munich, Germany, [6]Department of Physical Geography and Ecosystem Science, Lund University, Lund, Sweden

It is reported that the China–Pakistan Economic Corridor has been affected by extreme precipitation events. Since the 20th century, extreme weather events have occurred frequently, and the damage and loss caused by them have increased. In particular, the flood disaster caused by excessive extreme precipitation seriously hindered the development of the human society. Based on CRiteria Importance Through Intercriteria Correlation and square root of generalized cross-validation, this study used intensity–area–duration to analyze the trend of future extreme precipitation events, corrected the equidistance cumulative distribution function method deviation of different future scenario models (CESM2, CNRM-CM6-1, IPSL-CM6A-LR, and MIROC6) and evaluated the simulation ability of the revised model. The results showed that: 1) the deviation correction results of CNRM-CM6-1 in the Coupled Model Intercomparison Project Phase (CMIP) 6 could better simulate the precipitation data in the study area, and its single result could achieve the fitting effect of the CMIP5 multimodel ensemble average; 2) under CNRM-CM6-1, the frequency of extreme precipitation events under the three climate scenarios (SSP1-2.6, SSP3-7.0, and SSP5-8.5) presents interdecadal fluctuations of 3.215 times/10A, 1.215 times/10A, and 5.063 times/10A, respectively. The average impact area of extreme precipitation events would decrease in the next 30 years, while the total impact area and the extreme precipitation events in a small range would increase. Under the future scenario, the increase rate of extreme precipitation was highest in August, which increased the probability of extreme events; 3) in the next 30 years, the flood risk had an obvious expansion trend, which was mainly reflected in the expansion of the area of high-, medium-, and low-risk areas. The risk zoning results obtained by the two different flood risk assessment methods were different, but the overall risk trend was the same. This study provided more advanced research for regional flood risk, reasonable prediction for flood risk under future climate models, and useful information for flood disaster prediction in the study area and contributes to the formulation of local disaster prevention and reduction policies.

Keywords: China–Pakistan economic corridor, precipitation extremes, IAD, future scenarios, flood risk

1 INTRODUCTION

The impact of climate change on the hydrological cycle has been recognized for a long time (Sun et al., 2021). Although it is widely acknowledged that precipitation extremes are likely to cause an increase in flood risk, the relationship between climate and flood is rather complex (Zhang et al., 2008). It was reported that frequent extreme climate events had brought the serious loss of life and property to people worldwide since the beginning of the 21st century (Zhang et al., 2011). With the increasing emissions of global carbon dioxide and other greenhouse gases, global warming continues to intensify (Pachauri and Reisinger, 2008; Huang et al., 2017), and the instability and extremes of the climate increased, increasing the intensity and frequency of extreme precipitation events and floods in the future scenario (Meehl et al., 2000). Floods caused by extreme precipitation frequently occur in China-Pakistan Economic Corridor (CPEC) and increased frequency and strength with duration expansion. Therefore, it was urgently needed to investigate climate change's flood risk in high-risk areas.

Extreme precipitation events are critical indicators for studying extreme climate events and an essential factor for studying future climate changes. The flood disaster caused by extreme precipitation seriously hinders the development of society, and human civilization's progress has become the focus of attention all over the world (Goswami et al., 2006). In the present-day climate over most of the globe, the curve relating daily precipitation extremes with local temperatures had a peak structure, increasing as expected at the low–medium range of temperature variations but decreasing at high temperatures (Wang et al., 2011; Chang et al., 2022). Wang et al. (2015) attempted to explain the climate change effects on regional precipitation. However, the characteristics of precipitation extremes may depend on the method used for analysis. One method that could reveal precipitation characteristics is Intensity-Area-Duration (IAD), which for identifying extreme precipitation events was improved based on severity–Area–Duration (SAD) of Andreadis et al. (2005). This method was proved to be effective for assessing drought and flood risk by several researchers. Jing et al. (2016) applied IAD to identify regional extreme precipitation events for the first time in researching regional extreme precipitation events in China. They correlated the identified extreme precipitation events with population economic exposure. Wen et al. (2019) also used this method to identify drought events under three global warming scenarios based on several global climate models (CPEC (formerly known as silk road and well-known as Karakoram Highway) had been affected by extreme 25 precipitation events).

It should be noted that the role of precipitation extremes in shaping flood risk depends on land cover, region, and environmental conditions (Wang et al., 2017; Sun et al., 2022). Benito et al. (2015) used the flood risk assessment model established by the ancient flood data to assess the risk in Europe. The ancient flood data had a large time span and can fully reflect the impact of climate change. This kind of assessment method was more accurate in calculating flood probability. Yang et al. (2010) used the BP neural network algorithm of rough set reduction to obtain the flood risk. The integrated system based on the spatial processing ability of the geographic information system (GIS) has gradually become a powerful tool for flood risk assessment. Brendel et al. (2021) used SWMM and GSSHA to model storm pipeline networks and urban floods in Roanoke, Virginia. They found that the value of GSSHA to the city lies in its ability to predict flood duration and spatial range in a two-dimensional rangeability.

The GCMs were considered to be useful for the investigation of hydrological cycles (Li et al., 2018; Yang et al., 2021), decision-making in water resource management (Sun et al., 2021), and the atmosphere–land interactions (Simpkins, 2017; Sun et al., 2021). It may be helpful to use future scenarios and GCMs for the projection of precipitation extremes and flood risks (Su et al., 2008). The climate model was a vital tool used to predict climate change and explore the change mechanism of meteorological elements (Xue et al., 2013). At present, GCM simulations have provided climate change scenarios for scholars worldwide to carry out future climate research and evaluation and climate negotiations (Zhao et al., 2021). Regionalized increased and decreased drought duration and frequency were driven by changes in precipitation mean and variability (Su et al., 2006; Pierce et al., 2009; Sun et al., 2016). To predict the future flood risk of CPEC, provide theoretical support for managers to formulate policies, and reduce the losses caused by extreme events in CPEC, this study used IAD to predict the trend of future extreme precipitation events based on the data on three new combined path models in CMIP6. In addition, it used four future scenario model data sets to predict future extreme events. The results were analyzed and compared by downscaling analysis. Then, the most suitable model for CPEC was selected to obtain the development trend of flood disaster risk of CPEC and provide theoretical support for future risk aversion. The rest of this article describes the data and methods in **Section 2**. The results are presented in **Section 3**, followed by discussions in **Section 4** and conclusions in **Section 5**. This study will provide a reference for the research of regional flood risk and the prediction of regional flood risk under future scenarios and provide theoretical support for extreme regional events and flood prevention measures.

2 DATA AND METHODS

2.1 Study Area

CPEC extends from the port of Guarda in Pakistan to Kashgar in China, especially covering the whole territory of Pakistan, Kashgar in Xinjiang, and its surrounding areas, with a total length of about 3,000 km and a total area of about 932,000 km^2. The Indus River is an international river that runs through the whole territory of Pakistan and provides most of the irrigation water in the region. Its five tributaries, Jhelum River, Janab River, Ravi River, Bias River, and Sutlej River, converge in the Punjab plain (**Figure 1**). The precipitation in CPEC was mainly affected by two weather systems: summer precipitation and winter precipitation (Khan et al., 2014). Summer precipitation resulted from the Indian Ocean

TABLE 1 | Basic information of four global climate models in CMIP6.

Model	Institution	Resolution (longitude × latitude)	Ensembles
CESM2	NSF-DOE-NCAR	1.25 × 0.9424	r1i1p1f1
CNRM-CM6-1	CNRM-CERFACS	1.4062 × 1.4088	r1i1p1f2, r2i1p1f2, r3i1p1f2, r4i1p1f2, r5i1p1f2, and r6i1p1f2
IPSL-CM6A-LR	IPSL	2.5 × 1.2676	r1i1p1f1
MIROC6	MIROL	1.4062 × 1.4088	r1i1p1f1

monsoon disturbance, and winter precipitation resulted from the Mediterranean westerly disturbance (Safi et al., 2018). The southern part of CPEC was affected by the Indian Ocean monsoon climate with uneven precipitation and regional precipitation within the year, which was very prone to extreme precipitation. Since the 1990s, the precipitation in this area has increased significantly, and extreme climate events have been significant. Flash floods, originating from extreme weather events, have relatively less duration but severe intensity and impacts. These floods usually occur during the South Asian monsoon period between July and September (Memon et al., 2015). In 2011, large-scale heavy rains were observed in Sindh, leading to substantial economic losses, destruction of ecological resources, food shortages, and starvation (Haq et al., 2012).

Historically, CPEC has suffered many rainstorms and flood disasters (Federal Flood Commission, Ministry of Water and Power, 2015). According to statistics, 25 significant flood events have occurred in CPEC in the past 70 years. The flood disaster had caused more than $30 billion in the loss in Pakistan. About 25,502 people were killed, 197,273 villages were destroyed, 616,598 km^2 of land has been affected, and the flood disaster has become one of the main challenges affecting local economic and social development.

2.2 Data
2.2.1 Precipitation Data Sets
This study used a specific precipitation data set to study and analyze the extreme precipitation events and flood risk assessment. This data set used the professional meteorological interpolation software ANUSPLIN to carry out spatial interpolation combined with three-dimensional geospatial information and evaluate the interpolation model's effect through generalized cross-validation and error analysis. Test and verification of this data set can be referred to Wu et al. (2021).

The CMIP6 precipitation data were selected for this study's extreme precipitation and flood risk projection. Compared with the planned model, the scenario model in CMIP6 usually had better resolution and improved dynamic process, and the new emission scenario based on the shared socioeconomic pathway (SSP)/Representative Concentration Pathways (RCP) could be used for future climate change simulation (Eyring et al., 2016; O'Neill et al., 2016; Riahi et al., 2017; Jiang et al., 2020). The models data used in this study were three scenarios (SSP1-2.6, SSP3-7.0, and SSP5-8.5) of the global climate model (**Table 1**) in the scenario comparison plan under CMIP6. The precipitation data from 1984 to 2013 were used as the base period, and the data from 2021 to 2050 were used as the simulation data. In order to

facilitate comparative analysis, based on the observation data set, the spatial resolution of model data was uniformly interpolated on a grid point of 0.25 × 0.25 by bilinear interpolation. The data used in the grid include the data on 50 meteorological stations within CPEC. The stations are evenly distributed in the south of 30°N, relatively concentrated in 30°N ~ 35°N, and almost no stations are distributed in the north of 35°N in the study area. According to the precipitation distribution in the study area, the area north of 35°N is affected by terrain and airflow, and the annual precipitation is sparse, so it can be ignored. The precipitation in the whole study area is mainly distributed in the southern and central plains. Therefore, the selection of sites is reasonable.

Notably, the daily scale data are more obvious than the monthly scale data. We had considered using daily scale data to make the results of the benchmark period close to the extreme situation. However, the data on the benchmark period here was mainly to verify the relative accuracy of the model simulation and select the best. Therefore, the data on the monthly scale could fully achieve the purpose here. We also referred that Ali et al. (2018) used Hydrologiska Byrans Vattenbalansavdeling (HBV) light model to simulate the hydrology of the Hunza River Basin, which is affected by extreme precipitation. It was found that the model based on monthly scale data performs better. Based on this, they compared the simulation results of CSM1.1, CanESM2, and MIROC-ESM three GCMs models in the future scenario.

Here, this study selected four different model data recently released by CMIP6 for long-term simulation ability evaluation and set the model data closest to the measured data for statistical downscaling to improve the simulation ability of the model further (Lu et al., 2021). These models were commonly used by others. Abbas et al. (2022) used these four models for climate simulation in Pakistan. The CESM2 simulations exhibit agreement with satellite-era observations of the climate mean state, seasonal cycle, and interannual variability that are among the closest coupled climate model in the present CMIP6 archive (Danabasoglu et al., 2020). The equilibrium climate sensitivity of CNRM-CM6-1 is significantly increased compared to that of CNRM-CM5-1 (Voldoire et al., 2019). The equilibrium climate sensitivity and transient climate response of IPSL-CM6A-LR have increased from the previous climate model IPSL-CM5A-LR used in CMIP5 (Boucher et al., 2020). The tropical climate systems (e.g., summertime precipitation in the western Pacific and the eastward-propagating Madden-Julian oscillation) and the midlatitude atmospheric circulation (e.g., the westerlies, the polar
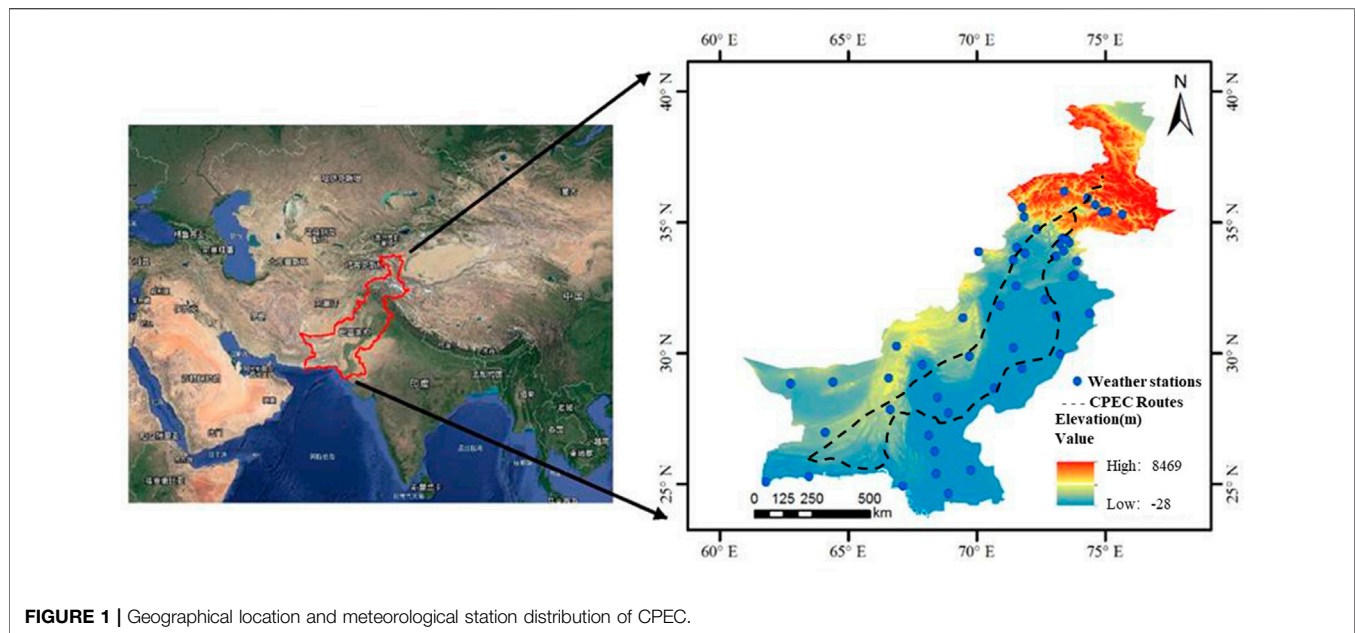
FIGURE 1 | Geographical location and meteorological station distribution of CPEC.

night jet, and troposphere–stratosphere interactions) are significantly improved in MIROC6 (Kataoka et al., 2020).

2.2.2 Collected Data for Flood Risk Assessment

The CPEC regional geographic data set was constructed in this study by comprehensively considering multiple data sources. The resampling method was used to solve the spatial data resolution difference between multiple data sources. The selected DEM data with 30 m resolution (downloaded from geospatial data cloud: http://www.gscloud.cn/) and the original DEM data processing were used to obtain non-depression DEM and slope data. The land use was divided into 10 categories (the impact of vegetation, water conservancy facilities, and other factors considered in the classification). Globeland30 (30M global surface coverage data, downloaded from the National Geographic Information Resources Directory Service System: https://www.webmap.cn/) was used to sort according to the impact degree, and the partial area index of the cultivated land was obtained after processing. The NDVI indexes required for analysis were obtained from landsat8 satellite data through image processing and band operation. Furthermore, the gridded population of the world (GPW) V4 population density data set (grid 0.25°, 30 km resolution) was selected to obtain the population density data in the study area. In order to get the building density, this study used the 2010 QuickBird orthophoto of CPEC as the primary data source. The road network density map was drawn after the aforementioned parallel processing based on the road network data (from OpenStreetMap: https://www.openstreetmap.org/).

2.3 Methods
2.3.1 Intensity–Area–Duration (IAD)

By employing IAD, this study comprehensively considered the three-dimensional characteristics, which was the intensity, impact area, and duration of extreme precipitation, and defines the grid set with certain intensity within a specific range on a given timescale as an extreme precipitation event based (Andreadis et al., 2005) on drought SAD.

In identifying extreme precipitation events, we first extracted the scope of the event, that is, the influence area of an extreme precipitation event. The grid point with the largest relative intensity within the range of extreme precipitation events in each timescale was the "strongest precipitation center" of the event, and then we searched the "secondary heavy precipitation center" from the center to the surrounding and repeated until there was no point exceeding the threshold within the range. Each extreme precipitation event's relative intensity and impact area was recorded, and then we found a new "strongest precipitation center" and repeated the aforementioned steps until all regional extreme precipitation events within the duration scale were found (**Figure 2**).

2.3.2 Assessment of the Flood Risk

The intuitionistic fuzzy analytic hierarchy process (IFAHP) was an improved subjective weighting method based on the analytic hierarchy process (AHP) (Sadiq and Tesfamariam, 2009). First, the intuitionistic fuzzy judgment matrix was constructed, and then its consistency was tested, and finally, the weight of each index was calculated.

CRITIC was an objective weighting method proposed by Diakoulaki et al. (1995). The basic idea of determining the index weight was based on two fundamental concepts: one was a comparative strength, and the other was the conflict between indicators. The basic idea of the critical method was to comprehensively use the difference and disagreement between indicators to calculate the weight, and the difference was based on the standard deviation σ. The calculation formula was as follows:

FIGURE 2 | Schematic diagram of identifying extreme precipitation events by the IAD method. **(A)** Distribution map of extreme precipitation events in different duration scales in the region. **(B)** Calculation steps of IAD identifying extreme precipitation events, which includes cyclic judgment calculation. The extreme precipitation events within the range are gradually identified according to the intensity until all identification is completed, and finally, the IAD envelope is obtained.

$$\sigma = \sqrt{\frac{1}{n}\sum_{i=1}^{n}\left(X_i - \bar{X}\right)^2}, \qquad (1)$$

where n is the evaluation quantity of the same index, X_i is the ith value of the same index, and $\bar{X}$ is the average value of the index value.

The improved combination weighting method of game theory (ICWGT) analyzed the rationality and decision equilibrium of decision-making behavior when game theory interacts with each other by introducing game theory in the field of operations research. Its idea of combination weighting was to find a consistent or compromise weighting method among different weighting methods by minimizing the deviation between each index weight and the optimal linear combination index weight to achieve a balanced optimization method (Ren and Li, 2017) to screen the optimal combination weight. The combination weighting based on game theory could be expressed as follows:

$$w = \sum_{l=1}^{L}\alpha_l w_l^T, \qquad (2)$$

where α_l is the linear combination coefficient, $\alpha_l > 0$, w is the combined weight vector, and w_l is the weight obtained by each weighting method. The weight vector w is combined with all w_l values; the objective was to minimize the deviation of L. By optimizing the L linear combination coefficients of the

aforementioned formula, the optimal solution w^* of w can be obtained. The resulting game model was as follows:

$$min\left\|\sum_{l=1}^{L}\alpha_l w_l^T - w_p\right\|_2, p = 1, 2..., L, \qquad (3)$$

where p indicates the number of methods to calculate the weight of evaluation indicators, and the pth basic weight set is w_p.

In this study, the index weight of subjective weighting was obtained according to IFAHP, and the index weight of objective weighting was obtained according to CRITIC. On the basis of these, the combination coefficient was calculated through the improved game theory combination weighting, and the final index weight with combination weighting was normalized. Details of the process can be referred to Wu et al. (2021).

2.3.3 Accuracy Assessment

The global model data would inevitably appear in the simulation of regional precipitation, and there would be corresponding deviations in interpolating the grid data. To improve the simulation accuracy of the model data, a statistical downscaling correction method was used for model correction. Statistical downscaling of climate models was carried out through EDCDFm. It corrected the deviation of GCM-simulated climate elements through the difference of cumulative distribution

characteristics between measured data and GCM-simulated data to make the model achieve a more accurate simulation effect. It was assumed that the difference between the cumulative distribution probabilities of the two data in the observation stage would remain unchanged in the future.

$$F(x) = (1 - Q)H(x) + G(X), \quad (4)$$

where $F(x)$ is the cumulative distribution function of precipitation in the observation period, and q is the proportion of precipitation months. $H(x)$ is the step function. The month without precipitation is 0, and the month with precipitation is 1.

$$P_{mcf} = F_{OC}^{-1}(F_{mc}(P_{mc})), \quad (5)$$

$$P_{mpj} = P_{mp} \frac{F_{oc}^{-1}\left(F_{mp}\left(P_{mp}\right)\right)}{F_{mc}^{-1}\left(F_{mp}\left(P_{mp}\right)\right)}, \quad (6)$$

where P_{mcj} is the corrected value of the model data in the base period, P_{mpj} is the corrected value of the model data in the future period, F_{oc}^{-1} is the quantile function of the observed value in the base period, F_{mc} is the cumulative distribution function in the historical period of the model, P_{mc} is the precipitation data in the historical period of the model, P_{mp} is the precipitation data simulated in the future of the model, and F_{mc}^{-1} is the quantile function in the historical period of the model, and F_{mp} is the cumulative distribution function of data in the future period of the model.

RTGCV was selected to compare and analyze the model interpolation results with the observed values and combined with the root mean square error (RMSE) as the index to evaluate the interpolation effect. RMSE was the estimated value error after excluding the observed value error. The smaller the RMSE was, the better the interpolation effect was. Through verification, it was found that the fluctuation of RTGCV had apparent periodic law, with larger in summer and less in autumn and winter, and there were no significant interannual variation characteristics.

3 RESULTS

3.1 Data Accuracy Assessment in CPEC

For the validation of observed precipitation data sets used in this study, the statistical analysis showed that the annual average RMSE of interpolation grid point was 0.9 mm, which showed that the precipitation grid-point data had good accuracy and interpolation effect. The precipitation data obtained by GCMs were then compared with observed data sets. First, the simulation ability of the four models' data interpolated to the same accuracy was evaluated. Then, the multiyear average monthly precipitation was used as the evaluation index.

According to the existing research, the precipitation seasons in CPEC are from July to September. In particular, there are many extreme precipitation events in August, and the probability of extreme precipitation events will increase in the future (Bhatti et al., 2020). Therefore, the results obtained from the accurate

evaluation of the model in August are more reasonable and representative. Consequently, the data of a grid point in August were taken as an example.

Figure 3A showed that the rainfall after correction matches well, which significantly reduced the correction error; **Figure 3B** showed the measured multiyear average monthly precipitation in the benchmark period 1984–2013 and the multiyear average monthly precipitation in the historical period of model simulation. It could be seen that except that MIROC6 obviously underestimates precipitation; most of the precipitation simulated by other models was slightly overestimated. Among them, the precipitation simulated by CNRM-CM6-1 was slightly underestimated by 10 mm in July, and the rest was overestimated somewhat, and its simulation situation was the closest. On the other hand, IPSL-CM6A-LR had the best simulation effect in March and May, and several models had significantly overestimated the simulation in November. In **Figure 3C**, the Taylor diagrams of four models were given, and the results of several models were in a good interval, among which CESM2 and CNRM-CM6-1 had smaller RMSD (Equivalent to RMSE divided by the standard deviation of the observed data).

Here, CESM2 and CNRM-CM6-1 with better precipitation simulation effect were selected for EDCDFm deviation correction, the simulation ability of the revised model was evaluated, and the Taylor diagram was used to compare the proximity between the two models and the observation data. The results of the model evaluation are shown in **Figure 3D**. Among them, the spatial correlation coefficients of the two corrected models were more outstanding than 0.9, the RMSD of CNRM-CM6-1 was smaller, and the ratio of their standard deviation was close to 1. Therefore, the model data simulation ability of CNRM-CM6-1 were more robust, and the three paths of the model data were selected for extreme precipitation event evaluation.

3.2 Projection of Extreme Precipitation in CPEC

For extreme precipitation events in different durations, the frequency difference of extreme precipitation events in the three scenarios in the future was not obvious under the condition of continuous 3d extreme precipitation.

Figure 4 shows the frequency of extreme precipitation events in the three scenarios in the future. The years of maximum frequency indicated under the three scenarios were different. Under SSP3-7.0, the frequency of extreme precipitation was the highest around 2037, and SSP1-2.6 was consistent with the year of the maximum frequency of extreme precipitation under SSP5-8.5. After reaching the maximum frequency, it showed a downward trend and then rose again after reaching the bottom in 2046. From the overall direction, under the three scenarios, the frequency of extreme precipitation fluctuated and increased and increased significantly in 2030. The interdecadal frequency variabilities under the three scenarios were 3.215 times/10A, 1.215 times/10A, and 5.063 times/10A, respectively. The interdecadal variability of extreme precipitation under the three scenarios was quite different. The

FIGURE 3 | (A) Model correction process (Taking August data of a grid point as an example). **(B)** Monthly precipitation in the base period and the monthly precipitation simulated by the model data. **(C)** Taylor diagram of four model data. **(D)** Taylor diagram of the model after deviation correction.
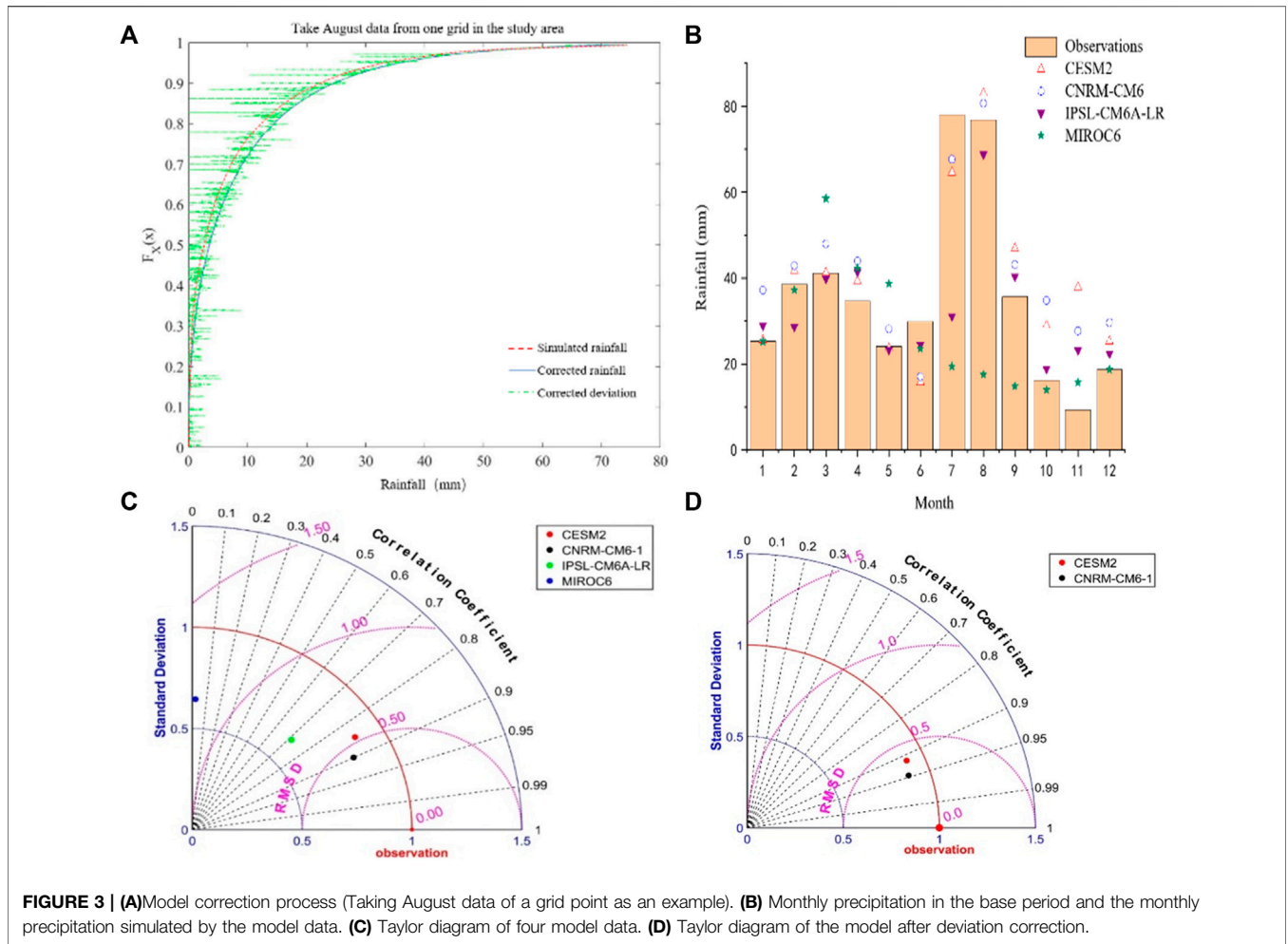
interdecadal variability under SSP5-8.5 was relatively large, in line with the climate change characteristics of high forcing and high radiation.

Comparing the occurrence of extreme precipitation events in the prediction stage with the average extreme precipitation frequency in the reference period, **Figure 5** was obtained. Compared with the base period, the extreme precipitation frequency under the three scenario models showed an upward trend, with significant extreme points under SSP1-2.6 and a large variation range under SSP3-7.0. On the other hand, under SSP5-8.5, the change of extreme precipitation frequency was relatively average, but it was always a large stage.

The impact area of extreme precipitation events was the grid area covered by an extreme event, and it was one of the important indicators to evaluate extreme precipitation events. In the prediction period, the average annual impact area under the three scenarios of extreme precipitation events lasting for 1 day generally showed an upward trend year by year (**Figure 6**). Among them, the impact area under SSP5-8.5 increased the fastest, and the minimum area exceeded 20000 km^2, the multiyear average impact area of a single event was 41000 km^2, and the maximum impact area reached 52.53 million km^2. As a result, the total impact

area in the prediction period was 120.33 million km^2, and the total impact area in the benchmark period was 101.44 million km^2.

In **Figures 4–6**, we concluded that in the next 15 years, the average impact area of extreme precipitation events under the three scenarios would decrease, and the total impact area would increase to a certain extent. In addition, the number of extreme events would decrease slightly, indicating that the number of small-scale and high-intensity extreme precipitation events would increase from 2021 to 2035. In the next 30 years, the average impact area of extreme precipitation events would decrease, the total impact area would increase, and the number of extreme events would increase, indicating that the number of small-scale extreme precipitation events would increase from 2021 to 2050.

The observation of precipitation extremes was largely different among different SSPs. In identifying IAD extreme precipitation events, this study adopts the concepts of grid precipitation threshold and relative intensity. Most of the grid precipitation thresholds have increased in varying degrees under the following three scenarios, especially for periods of 5 days and 7 days. The multiyear monthly average precipitation was used as the standard to obtain the
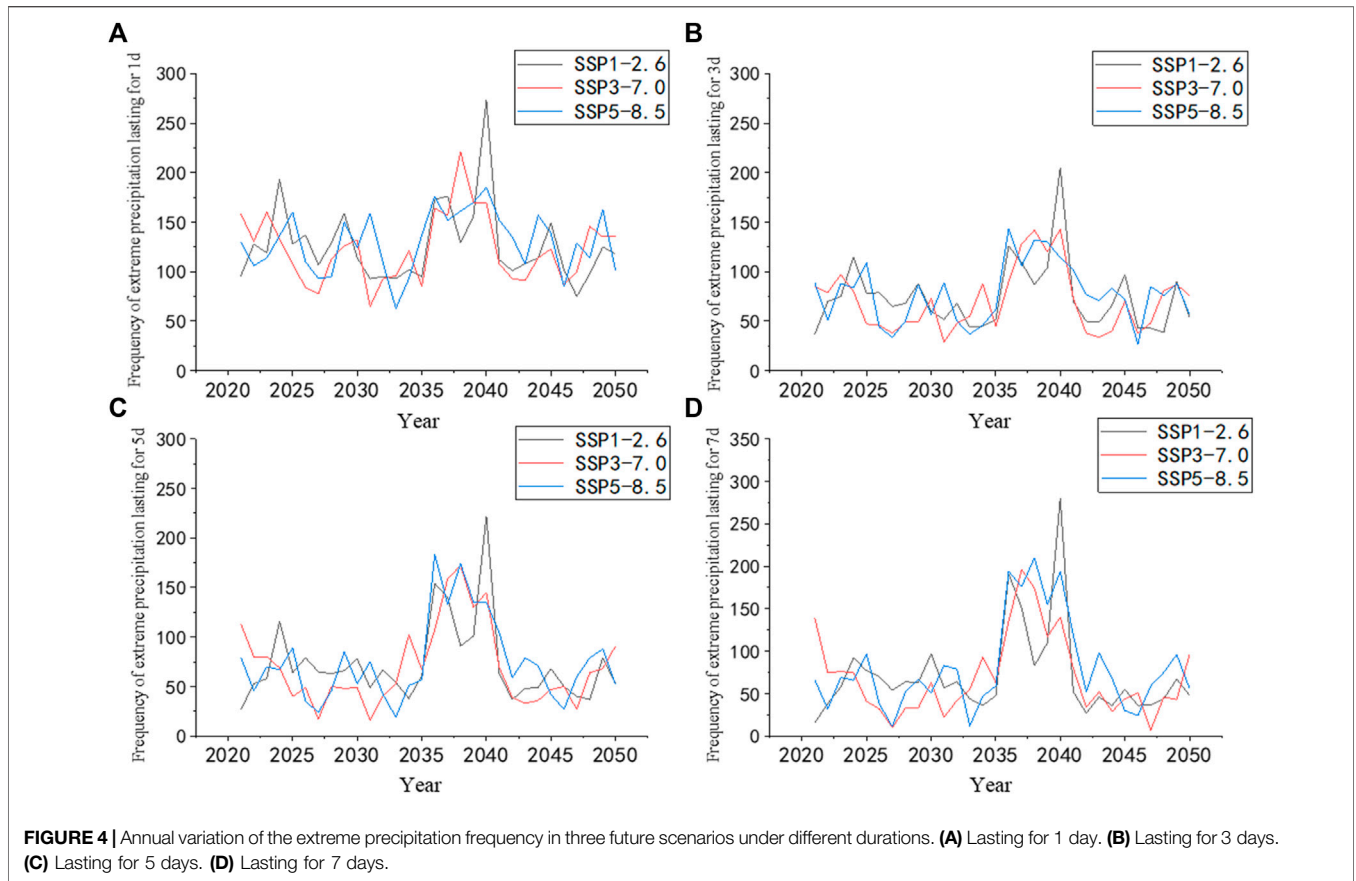
FIGURE 4 | Annual variation of the extreme precipitation frequency in three future scenarios under different durations. **(A)** Lasting for 1 day. **(B)** Lasting for 3 days. **(C)** Lasting for 5 days. **(D)** Lasting for 7 days.
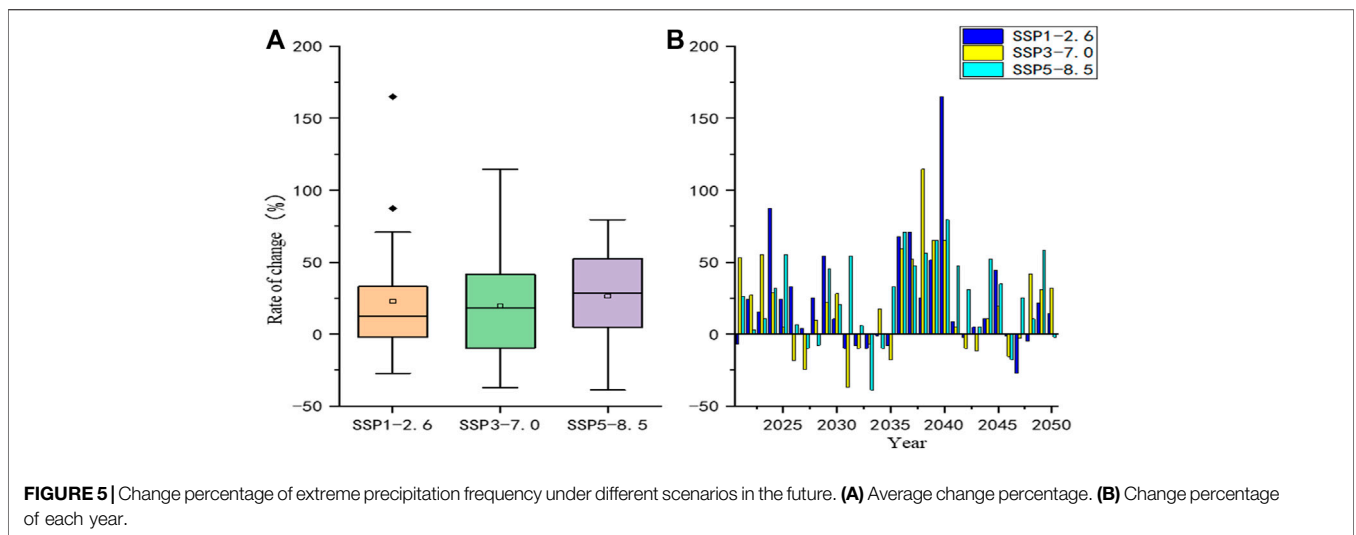
FIGURE 5 | Change percentage of extreme precipitation frequency under different scenarios in the future. **(A)** Average change percentage. **(B)** Change percentage of each year.

variation trend of future precipitation. **Figure 7** shows the multiyear average monthly precipitation during the observation period from 1984 to 2013 and the future three scenarios from 2021 to 2050. For the dry season, the precipitation under SSP1-2.6 was more than that under other paths, and the simulation of precipitation in SSP1-2.6 focused on balancing the precipitation in the dry season; In the

rainy season (July/August), the simulation under SSP5-8.5 was more significant than the other two. This was a precipitation process simulated by high radiation and high forcing without climate policy intervention, which could better represent an extreme scenario. Therefore, the following inundation simulation and flood risk assessment were carried out using the precipitation data under this scenario.

FIGURE 6 | Average annual impact area of extreme precipitation under different scenarios in the future. **(A)** Under SSP1-2.6. **(B)** Under SSP3-7.0. **(C)** Under SSP5-8.5.

FIGURE 7 | Monthly average precipitation in the base period and monthly average precipitation in three combined paths from 2021 to 2050.
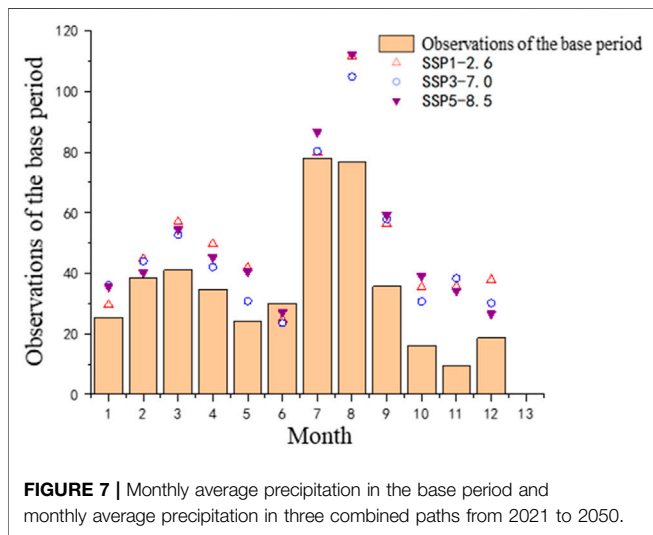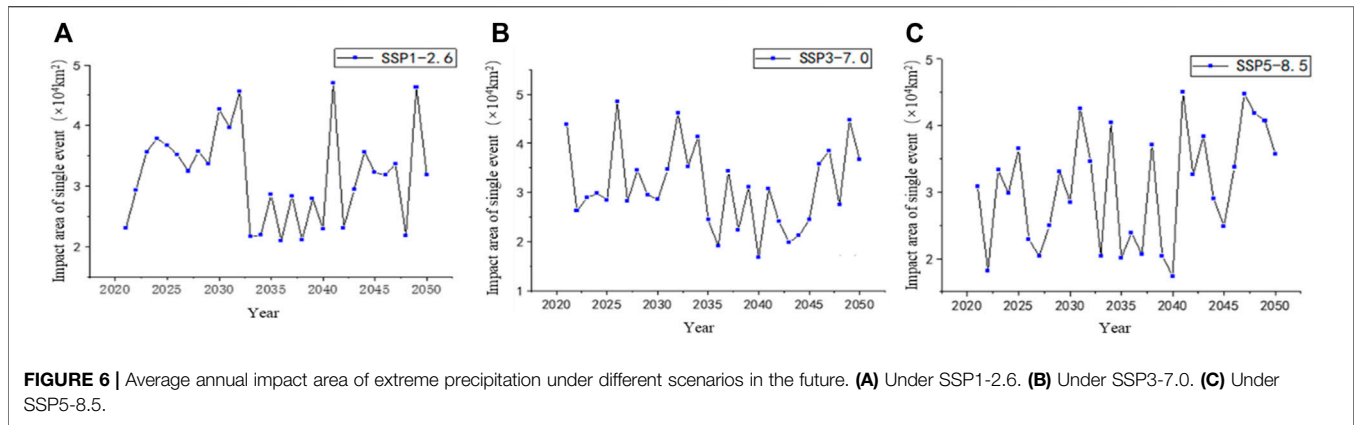
3.3 Projection of the Flood Risk in CPEC

In the context of global climate change, the intensity of extreme precipitation was increasing. Through the processing and research of model data, this study obtained that the extreme precipitation was the most obvious under SSP5-8.5. Therefore, the daily rainfall value in 2021–2050 under SSP5-8.5 and CNRM-CM6-1 was selected to calculate the area rainfall process with a 100-year return period and 20-year return period, and the corresponding DEM, land use, and other data were substituted into the flood area model for simulation, The flood inundation map (**Figure 8**) of the 100-year return period (high scenario) and 20-year (low scenario) under the future climate model scenario could be obtained to guide the flood prevention work under the future climate change scenario.

As shown in the figures, compared with the design flood inundation distribution in the historical period, the design flood inundation range had a partial increasing trend in the

FIGURE 8 | Schematic diagram of the flood risk under the future scenario (SSP5-8.5). **(A)** 100-year flood process value. **(B)** 20-year flood process value.

FIGURE 9 | Flood risk zoning in different return periods under future scenarios (SSP5-8.5). **(A)** 20-year flood risk zoning. **(B)** 100-year flood risk zoning.
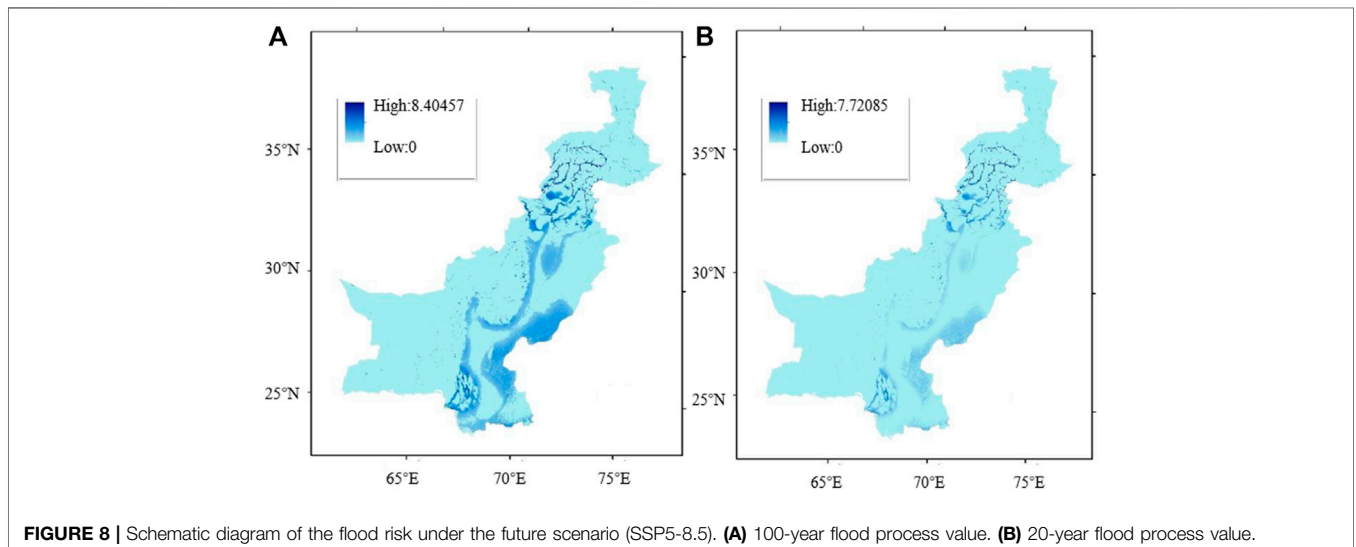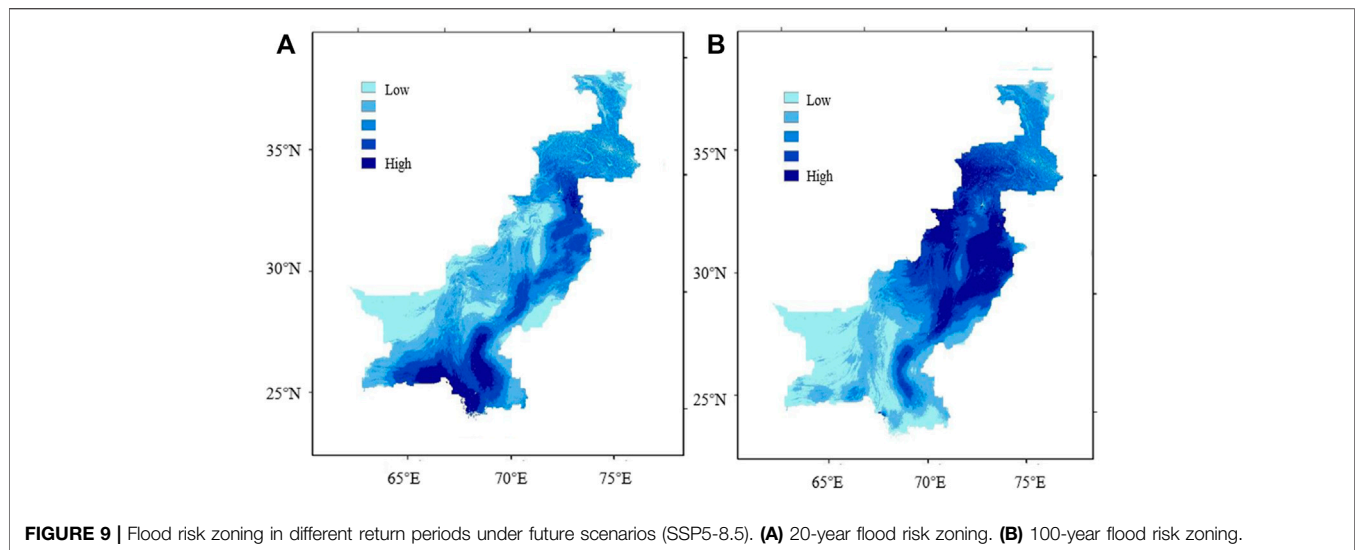
future scenario and had increased in a small range. According to the statistics of inundation areas in different water depths, it was found that the increased range of inundation areas in different risk areas was different. Compared with the flood inundation in the historical period, the expansion area of the design 100-year flood under 1 m inundation depth was more prominent in the future scenario, and the expansion area of high water depth inundation was less pronounced.

As for frequency calculation, the daily rainfall data from 2021 to 2050 under SSP5-8.5 and CNRM-CM6-1 were selected for analysis. The grid-point rainfall was calculated as the design rainfall under the return period of 20 years and 100 years, respectively. The spatial distribution of design rainfall was obtained by interpolation of design rainfall to carry out the following risk assessment calculation. Finally, the 20-year flood risk distribution and 100-year flood risk distribution under the future scenario could be obtained (**Figure 9**). Compared with the historical observation period, under the future scenario, the area of medium- and high-risk areas in the 20-year flood risk zoning was partially expanded, especially located in the south of Sindh province and part of the Indus River into the sea, and the medium- and high-risk areas tend to expand in the middle of Punjab province. The expansion of the high-risk area with 100-year flood risk was the most obvious, which was mainly located in the plain of Punjab province. The area of the high-risk area was expanded by about 3.1%. The area of the low-risk area was in the south of Sindh province, and the south of Balochistan province had increased by 4.2%, and the area of the low-risk area and the medium-risk area had decreased correspondingly.

In general, the area of high-risk areas in the future scenario had an expanding trend, especially located in the east and south, affected by the summer monsoon and densely populated areas. Therefore, it was necessary to improve the flood prevention level further to avoid more significant losses in the future.

4 DISCUSSION

Due to the differences in simulation mechanism, topographic elements, and spatial resolution of different climate models, the simulation results were uncertain, and the simulation ability of other regions was different, especially in areas with complex topographic and atmospheric elements. The prediction of global precipitation data by the model data before CMIP5 was more in line with the measured situation than in a single region. In recent years, significant progress has been made in the regional simulation of GCMs. Huang et al. (2015) found that CMIP5 multimodel set data had a strong simulation ability for temporal and spatial temperature and precipitation changes. The model could also well simulate the seasonal fluctuations of precipitation. Chen et al. (2014) used 43 GCMs to predict the precipitation in China. They found that the CMIP5 model data could better simulate the regional distribution characteristics, which were higher in the southwest. Therefore, when using the global climate model to analyze the various features of meteorological elements under regional future climate change, it was necessary to select appropriate GCMs and evaluate the simulation ability of the climate model. Significantly, there would still be uncertainty in the application of GCM in predicting extreme regional events even if there were downscaling methods and deviation correction methods and the RCM dynamical downscaling method was still dominant in terms of regional precipitation simulation (Guo and Wang, 2016). In future research, it is suggested to use RCM or the GCM model with high accuracy and project precipitation extremes/floods.

Unlike CMIP5 model data, CMIP6 combined the typical concentration path and shared economy path to form a new scenario path model (SSP-RCP) to obtain more reliable prediction results. Jiang et al. (2020) also attempted to use CMIP6 data to evolve temporal–spatial characteristics of temperature and precipitation. However, IAD was not applied to their study. The climate in different regions of CPEC was quite different. Therefore, it was difficult to study the change

characteristics of extreme events in time series on a large unified scale and take the characteristics of different regions into account. The study area could be divided according to climatic and topographic characteristics to further explore the changing trend of extreme events in different regions. Spatially, the number of people affected by drought would be greater than that in the reference period. The increase in temperature exacerbated the drought. Regional drought risk levels were different (Wen et al., 2019), which proved IAD had a good effect on spatial characteristics. Considering the three-dimensional aspects of extreme precipitation events, IAD clustering was used to identify extreme precipitation events in CPEC in this study. The changing trend of extreme precipitation events under the background of climate change was obtained. It could expand the simulation path of the existing research to carry out more representative research on extreme climate events.

In this study, the newly released model data in CMIP6 were downscaled, the simulation ability was evaluated, and the applicability of CNRM-CM6-1 model data in CPEC was obtained. Compared with CMIP5, the single CNRM-CM6-1 model in CMIP6 could achieve the fitting effect of the multimodel aggregation average in CMIP5. Furthermore, the path data of three SSPs under CNRM-CM6-1 in CMIP6 were used to predict and evaluate extreme events under different climate change backgrounds in the future. Meanwhile, IFAHP, CRITIC, and ICWGT used in this study for assessing flood risk could make results obtained quickly, which was helpful for the division of flood risk areas. In previous studies, Abbas et al. (2022) found that under the high-forcing scenario (SSP5-8.5), the trend of extreme precipitation events in CPEC increased significantly, and the tendency of extreme precipitation events in summer also increased significantly, which is consistent with the conclusions of this article. In the verification of temperature simulation in Thailand (Suchada et al., 2021), the simulation results and accuracy of CNRM-CM6-1 were affirmed, so the accuracy of the simulation results based on CNRM-CM6-1 could be considered to be guaranteed. However, the resolution of CNRM-CM6-1 may still impact the accuracy of research results. Therefore, in future research, if the model's resolution can be solved, it will be an important breakthrough in improving the accuracy of disaster prediction.

5 CONCLUSION

For the rainfall data under the new combination scenario in the newly released CMIP6 model data, EDCDFm was used to correct the downscaling deviation. Before the correction, the model data were partially overestimated for rainfall. We selected the model closest to the measured data for correction. The single corrected model had a good fitting ability for the measured data's seasonal

fluctuation and spatial distribution. The appropriate level of a single model could reach the level of the multimodel set in CMIP5.

Variation characteristics of extreme precipitation events under the background of climate change. Under CNRM-CM6-1, the frequency of extreme precipitation events presents interdecadal fluctuations of 3.215 times/10A, 1.215 times/10A, and 5.063 times/10A under three combined path datasets (SSP1-2.6, SSP3-7.0, and SSP5-8.5). In the next 30 years, the average impact area of extreme precipitation events would decrease, the total impact area would increase, and the extreme precipitation events in a small range would increase. Under the future scenario, the increased rate of extreme precipitation in August was the fastest, which increased the probability of extreme events.

For the flood risk under different return periods in the future, compared with the observation period, the flood risk had a more obvious expansion trend in the next 30 years, which was mainly reflected in the expansion of the area of high-, medium-, and low-risk areas. The risk zoning results obtained by the two different flood risk assessment methods differed, but the overall risk trend was the same.

DATA AVAILABILITY STATEMENT

The original contributions presented in the study are included in the article/supplementary material; further inquiries can be directed to the corresponding authors.

AUTHOR CONTRIBUTIONS

Conceptualization, SD; data curation, RW; formal analysis, JX and WL; methodology, YT; resources, WZ; supervision, HS; validation, RW; writing—original draft, SD and RW; writing—review and editing, HS, SD, and DY. All authors have read and agreed to the published version of the manuscript.

FUNDING

REFERENCES

Abbas, A., Ullah, S., and Ullah, W. (2022). Evaluation and Projection of Precipitation in Pakistan Using the Coupled Model Intercomparison Project Phase 6 Model Simulations. *Int. J. Climatol.*, 1–20. doi:10.1002/joc.7602

Ali, A. F., Xiao, C.-D., Zhang, X.-P., Adnan, M., Iqbal, M., and Khan, G. (2018). Projection of Future Streamflow of the Hunza River Basin, Karakoram Range (Pakistan) Using HBV Hydrological Model. *J. Mt. Sci.* 15, 2218–2235. doi:10.1007/s11629-018-4907-4

Andreadis, K. M., Clark, E. A., Wood, A. W., Hamlet, A. F., and Lettenmaier, D. P. (2005). Twentieth-Century Drought in the

Conterminous United States. *J. Hydrometeorol.* 6 (6), 985–1001. doi:10.1175/jhm450.1

Benito, G., Macklin, M. G., Cohen, K. M., and Herget, J. (2015). Past Hydrological Extreme Events in a Changing Climate. *Catena* 130, 1–2. doi:10.1016/j.catena.2014.12.001

Bhatti, A. S., Wang, G., Ullah, W., Ullah, S., Fiifi Tawia Hagan, D., Kwesi Nooni, I., et al. (2020). Trend in Extreme Precipitation Indices Based on Long Term *In Situ* Precipitation Records Over Pakistan. *Water* 12, 797. doi:10.3390/w12030797

Boucher, O., Servonnat, J., and Albright, A. L. (2020). Presentation and Evaluation of the IPSL-CM6A-LR Climate Model. *J. Adv. Model. Earth Syst.* 12, e2019MS002010. doi:10.1029/2019MS002010

Brendel, C. E., Dymond, R. L., and Aguilar, M. F. (2021). Modeling Storm Sewer Networks and Urban Flooding in Roanoke, Virginia, with SWMM and GSSHA. *J. Hydrologic Eng.* 26 (1), 05020044. doi:10.1061/(asce)he.1943-5584.0002021

Chang, J., Gong, L., and Zeng, F. (2022). Using Hydro-Climate Elasticity Estimator and Geographical Detector Method to Quantify the Individual and Interactive Impacts on NDVI in Oasis-Desert Ecotone. *Stoch Stoch. Environ. Res. Risk Assess.*, 1–18. doi:10.1007/s00477-022-02184-4

Chen, X. C., Xu, Y., and Xu, C. H. (2014). Evaluation of CMIP5 Global Climate Model on Precipitation Simulation Ability in China. *Prog. Clim. Change Res.* 10 (03), 217–225. doi:10.3969/j.issn.1673-1719.2014.03.011

Danabasoglu, G., Lamarque, J.-F., and Bacmeister, J. (2020). The Community Earth System Model Version 2 (CESM2). *J. Adv. Model. Earth Syst.* 12, e2019MS001916. doi:10.1029/2019ms001916

Diakoulaki, D., Mavrotas, G., and Papayannakis, L. (1995). Determining Objective Weights in Multiple Criteria Problems: The Critic Method. *Comput. Operations Res.* 22 (7), 763–770. doi:10.1016/0305-0548(94)00059-h

Eyring, V., Bony, S., Meehl, G. A., Senior, C. A., Stevens, B., Stouffer, R. J., et al. (2016). Overview of the Coupled Model Intercomparison Project Phase 6 (CMIP6) Experimental Design and Organization. *Geosci. Model Dev.* 9 (5), 1937–1958. doi:10.5194/gmd-9-1937-2016

Federal Flood Commission, Ministry of Water and Power (2015). *Annual Flood Report 2015*. Islamabad (Pakistan): Government of Pakistan Ministry of Water and Power.

Goswami, B. N., Venugopal, V., Sengupta, D., Madhusoodanan, M. S., and Xavier, P. K. (2006). Increasing Trend of Extreme Rain Events Over India in a Warming Environment. *Science* 314 (5804), 1442–1445. doi:10.1126/science.1132027

Guo, D., and Wang, H. (2016). Comparison of a Very-Fine-Resolution GCM with RCM Dynamical Downscaling in Simulating Climate in China. *Adv. Atmos. Sci.* 33, 559–570. doi:10.1007/s00376-015-5147-y

Haq, M., Akhtar, M., Muhammad, S., Paras, S., and Rahmatullah, J. (2012). Techniques of Remote Sensing and GIS for Flood Monitoring and Damage Assessment: A Case Study of Sindh Province, Pakistan. *Egypt. J. Remote Sens. Space Sci.* 15 (2), 135–141. doi:10.1016/j.ejrs.2012.07.002

Huang, J. L., Su, B. D., and Zhu, X. Y. (2015). Simulation and Prediction of Climate Change in the Indus River Basin in South Asia by CMIP5 Multi-Model Set. *Glacial Permafr.* 37 (02), 297–307. doi:10.7522/j.issn.1000-0240.2015.0033

Huang, J., Zhang, X., Zhang, Q., Lin, Y., Hao, M., Luo, Y., et al. (2017). Recently Amplified Arctic Warming Has Contributed to a Continual Global Warming Trend. *Nat. Clim. Change* 7 (12), 875–879. doi:10.1038/s41558-017-0009-5

Jiang, T., Lv, Y. R., and Huang, J. L. (2020). Overview of CMIP6 Model New Scenario (SSP-RCP) and its Application in Huaihe River Basin. *Adv. Meteorol. Sci. Technol.* 10 (05), 102–109. doi:10.3969/j.issn.2095-1973.2020.05.016

Jing, C., Jiang, T., and Wang, Y. J. (2016). Study on Regional Extreme Precipitation Events and Population Economic Exposure in China. *J. Meteorol.* 74 (04), 572–582. doi:10.11676/qxxb2016.037

Kataoka, T., Tatebe, H., and Koyama, H. (2020). Seasonal to Decadal Predictions with MIROC6: Description and Basic Evaluation. *J. Adv. Model. Earth Syst.* 12, e2019MS002035. doi:10.1029/2019ms002035

Khan, S. I., Hong, Y., Gourley, J. J., Khattak, M. U. K., Yong, B., and Vergara, H. J. (2014). Evaluation of Three High-Resolution Satellite Precipitation Estimates: Potential for Monsoon Monitoring over Pakistan. *Adv. Space Res.* 54, 670–684. doi:10.1016/j.asr.2014.04.017

Li, H., Chen, H., Wang, H., and Yu, E. (2018). Future Precipitation Changes over China under 1.5 °C and 2.0 °C Global Warming Targets by Using CORDEX Regional Climate Models. *Sci. Total Environ.* 640-641, 543–554. doi:10.1016/j.scitotenv.2018.05.324

Lu, M., Sun, H., Yan, D., Xue, J., Yi, S., Gui, D., et al. (2021). Projections of Thermal Growing Season Indices over China under Global Warming of 1.5 °C and 2.0 °C. *Sci. Total Environ.* 781, 146774. doi:10.1016/j.scitotenv.2021.146774

Meehl, G. A., Karl, T., Easterling, D. R., Changnon, S., Pielke, R., Changnon, D., et al. (2000). An Introduction to Trends in Extreme Weather and Climate Events: Observations, Socioeconomic Impacts, Terrestrial Ecological Impacts, and Model Projections. *Bull. Amer. Meteor. Soc.* 81 (3), 413–416. doi:10.1175/1520-0477(2000)081<0413:aittie>2.3.co;2

Memon, A. A., Muhammad, S., Rahman, S., and Haq, M. (2015). Flood Monitoring and Damage Assessment Using Water Indices: A Case Study of Pakistan Flood-2012. *Egypt. J. Remote Sens. Space Sci.* 18 (1), 99–106. doi:10.1016/j.ejrs.2015.03.003

O'Neill, B. C., Tebaldi, C., van Vuuren, D. P., Eyring, V., Friedlingstein, P., Hurtt, G., et al. (2016). The Scenario Model Intercomparison Project (ScenarioMIP) for CMIP6. *Geosci. Model Dev.* 9 (9), 3461–3482. doi:10.5194/gmd-9-3461-2016

Pachauri, R. K., and Reisinger, A. E. (2008). *Climate Change 2007. Synthesis Report. Contribution of Working Groups I, II and III to the Fourth Assessment Report.* Geneva (Switzerland), Switzerland: IPCC.

Pierce, D. W., Barnett, T. P., Santer, B. D., and Gleckler, P. J. (2009). Selecting Global Climate Models for Regional Climate Change Studies. *Proc. Natl. Acad. Sci. U.S.A.* 106 (21), 8441–8446. doi:10.1073/pnas.0900094106

Ren, L. C., and Li, Z. F. (2017). A New Model Based on the Games Theory and Fuzzy Mathematics in Bridge Engineering Risk Assessment. *Highw. Eng.* 42 (1), 163–169. doi:10.3969/j.issn.1674-0610.2017.01.037

Riahi, K., van Vuuren, D. P., Kriegler, E., Edmonds, J., O'Neill, B. C., Fujimori, S., et al. (2017). The Shared Socioeconomic Pathways and Their Energy, Land Use, and Greenhouse Gas Emissions Implications: An Overview. *Glob. Environ. Change* 42, 153–168. doi:10.1016/j.gloenvcha.2016.05.009

Sadiq, R., and Tesfamariam, S. (2009). Environmental Decision-Making under Uncertainty Using Intuitionistic Fuzzy Analytic Hierarchy Process (IF-AHP). *Stoch. Environ. Res. Risk Assess.* 23 (1), 75–91. doi:10.1007/s00477-007-0197-z

Safi, U., You, Q. L., and Waheed, U. (2018). Observed Changes in Precipitation in China-Pakistan Economic Corridor during 1980–2016. *Atmos. Res.* 210, 1–14. doi:10.1016/j.atmosres.2018.04.007

Simpkins, G. (2017). Progress in Climate Modelling. *Nat. Clim. Change* 7 (10), 684–685. doi:10.1038/nclimate3398

Su, B. D., Jiang, T., and Dong, W. J. (2008). Statistical Fitting of Distribution Characteristics of Extreme Heavy Precipitation in the Yangtze River Basin. *Meteorol. Sci.* 28 (06), 625–629. doi:10.3969/j.issn.1009-0827.2008.06.006

Su, B. D., Jiang, T., and Ren, G. Y. (2006). Temporal and Spatial Variation Trend of Extreme Heavy Precipitation in the Yangtze River Basin from 1960 to 2004. *Prog. Clim. Change Res.* 2 (01), 9–14. doi:10.3969/j.issn.1673-1719.2006.01.002

Suchada, K., Pham, T. B. T., and Shabbir, H. G. (2021). Evaluation of CMIP6 GCMs for Simulations of Temperature Over Thailand and Nearby Areas in the Early 21st Century. *Heliyon* 7 (11), e08263. doi:10.1016/j.heliyon.2021.e08263

Sun, H., Bai, Y., Lu, M., Wang, J., Tuo, Y., Yan, D., et al. (2021). Drivers of the Water Use Efficiency Changes in China during 1982-2015. *Sci. Total Environ.* 799, 149145. doi:10.1016/j.scitotenv.2021.149145

Sun, H., Chen, L., Yang, Y., Lu, M., Qin, H., Zhao, B., et al. (2022). Assessing Variations in Water Use Efficiency and Linkages with Land-Use Changes Using Three Different Data Sources: A Case Study of the Yellow River, China. *Remote Sens.* 14 (5), 1065. doi:10.3390/rs14051065

Sun, W., Mu, X., Song, X., Wu, D., Cheng, A., and Qiu, B. (2016). Changes in Extreme Temperature and Precipitation Events in the Loess Plateau (China) during 1960-2013 under Global Warming. *Atmos. Res.* 168, 33–48. doi:10.1016/j.atmosres.2015.09.001

Voldoire, A., Saint-Martin, D., Sénési, S., Decharme, B., Alias, A., Chevallier, M., et al. (2019). Evaluation of CMIP6 DECK Experiments with CNRM-CM6-1. *J. Adv. Model. Earth Syst.* 11, 2177–2213. doi:10.1029/2019ms001683

Wang, D. G., Jiang, P., and Wang, G. L. (2015). Urban Extent Enhances Extreme Precipitation over the Pearl River Delta, China. *Atmos. Sci. Lett.* 16 (3), 310–317. doi:10.1002/asl2.559

Wang, G. L., Wang, D. G., and Kevin, E. T. (2017). The Peak Structure and Future Changes of the Relationships between Extreme Precipitation and Temperature. *Nat. Clim. Change* 7 (4), 268–274. doi:10.1038/nclimate3239

Wang, Y., Wan, Q., Meng, W., Liao, F., Tan, H., and Zhang, R. (2011). Long-term Impacts of Aerosols on Precipitation and Lightning over the Pearl River Delta Megacity Area in China. *Atmos. Chem. Phys.* 11, 12421–12436. doi:10.5194/acp-11-12421-2011

Wen, S. S., Wang, A. Q., and Tao, H. (2019). Population Exposed to Drought under the 1.5 °C and 2.0 °C Warming in the Indus River Basin. *Atmos. Res.* 218, 296–305. doi:10.1016/j.atmosres.2018.12.003

Wu, R. Y., Sun, H. W., and Yan, D. (2021). Evaluation of Flood Disaster Risk in China-Pakistan Economic Corridor by Combination Weighting Based on Improved Game Theory and Grid Data. *Trans. Chin. Soc. Agric. Eng. (Transactions CSAE)* 37 (14), 145–154. doi:10.11975/j.issn.1002-6819.2021.14.016

Xue, J. G., Mei, L. W., and Giorgi, F. (2013). Climate Change over China in the 21st Century as Simulated by BCC_ CSM1. 1-RegCM4. 0. *Atmos. Ocean. Sci. Lett.* 6 (05), 381–386. doi:10.1080/16742834.2013.11447112

Yang, L. C., Deng, S., and Xu, J. H. (2010). Flood Risk Assessment Algorithm Based on BP Network. *Comput. Technol. Dev.* 20 (04), 232–234. doi:10.3969/j.issn.1673-629X.2010.04.059

Yang, Y., Sun, H., Xue, J., Liu, Y., Liu, L., Yan, D., et al. (2021). Estimating Evapotranspiration by Coupling Bayesian Model Averaging Methods with Machine Learning Algorithms. *Environ. Monit. Assess.* 193, 156. doi:10.1007/s10661-021-08934-1

Zhang, L. P., Du, H., and Xia, J. (2011). Research Progress of Extreme Hydrological Events under Climate Change. *Prog. Geogr. Sci.* 30 (11), 1370–1379. doi:10.11820/dlkxjz.2011.11.006

Zhang, Q., Marco, G., and Chen, J. Q. (2008). Climate Changes and Flood/drought Risk in the Yangtze Delta, China, during the Past Millennium. *Quat. Int.* 176-177, 62–69. doi:10.1016/j.quaint.2006.11.004

Zhao, B. Q., Sun, H. W., and Yan, D. (2021). Quantifying Changes and Drivers of Runoff in the Kaidu River Basin Associated with Plausible Climate Scenarios. *J. Hydrol. Reg. Stud.* 38, 100968. doi:10.1016/j.ejrh.2021.100968